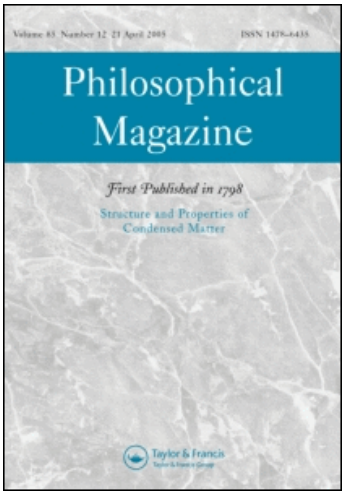

Philosophical Magazine
Publication details, including instructions for authors and subscription information:
http://www.informaworld.com/smpp/title~content=t713695589

Biomass and habitability potential of clay minerals- and iron-rich environments: Testing novel analogs for Mars Science Laboratory landing sites candidates

Rosalba Bonaccorsi[abc]; Christopher P. McKay[a]; Bin Chen[acd]
[a] Space Science and Astrobiology Division, NASA Ames Research Center, Moffett Field, CA 94035, USA [b] SETI Institute, Mountain View, CA 94043, USA [c] Advanced Studies Laboratories, NASA Ames, Moffett Field, CA 94035, USA [d] Department of Electrical Engineering, University of California, Santa Cruz, CA 95060, USA

Online publication date: 27 May 2010

To cite this Article Bonaccorsi, Rosalba , McKay, Christopher P. and Chen, Bin(2010) 'Biomass and habitability potential of clay minerals- and iron-rich environments: Testing novel analogs for Mars Science Laboratory landing sites candidates', Philosophical Magazine, 90: 17, 2309 — 2327
To link to this Article: DOI: 10.1080/14786435.2010.486374
URL: http://dx.doi.org/10.1080/14786435.2010.486374

Philosophical Magazine
Vol. 90, Nos. 17–18, 14–28 June 2010, 2309–2327

Taylor & Francis
Taylor & Francis Group

Biomass and habitability potential of clay minerals- and iron-rich environments: Testing novel analogs for Mars Science Laboratory landing sites candidates

Rosalba Bonaccorsi*[abd], Christopher P. McKay[a] and Bin Chen[acd]

[a]*Space Science and Astrobiology Division, NASA Ames Research Center, Moffett Field, CA 94035, USA;* [b]*SETI Institute, 515 N. Whisman Road, Mountain View, CA 94043, USA;* [c]*Department of Electrical Engineering, University of California, Santa Cruz, CA 95060, USA;* [d]*Advanced Studies Laboratories, NASA Ames, Moffett Field, CA 94035, USA*

(*Received 12 September 2009; final version received 14 April 2010*)

The landing site of the next mission to Mars (the US 2011 Mars Science Laboratory) will include phyllosilicate outcrops as targets for investigating the geological and biological history of the planet. In this context, we present a preliminary study assessing the living biomass and habitability potential in mineralogical Mars analogs by means of multi-component investigations (X-ray diffraction, microRaman spectroscopy and SEM\EDX). Phyllosilicate and hematite-rich deposits from the Atacama Desert (Chile), Death Valley (CA), and the California Coast, encompassing a broad arid to hyper-arid climate range (annual rainfall <0.2 to ~700 mm/year), were analyzed for total and viable Gram-negative biomass, i.e. adenosine 5′-triphosphate (ATP) and Limulus amebocyte lysate (LAL) assays. Basic observations were: (1) there is no systematic pattern in biomass content of clay-rich versus non-clay (oxidized) materials; (2) Atacama desiccation polygons (6.0×10^4 cells/g) and contiguous hematite-rich deposits contain the lowest biomass (1.2×10^5 cells/g), which is even lower than that of coarse-grained soil nearby ($3.3–5.0 \times 10^5$ cells/g); (3) the Atacama clay-rich samples (illite–muscovite and kaolinite) are three orders of magnitude lower than surface clay (montmorillonite, illite, and chlorite) from Death Valley; and (4) finally, and unexpectedly, the Gram-negative content ($\sim 6.4 \times 10^7$ cells/g) of clay mineral-rich materials from the arid Death Valley region is up to six times higher than that (~1.5 to $\sim 3.0 \times 10^7$ cells/g) of water-saturated massive clays (kaolinite, illite and montmorillonite) from the California Coast (wetter end-member). MicroRaman spectroscopy investigation on a Death Valley sample indicates that gypsum (1008, 618, and 414 cm^{-1} Raman shift), and inferred associated organic (scytonemin) biosignatures (1281 cm^{-1}) for the measured Gram-negatives (cyanobacteria) were successfully captured.

Keywords: phyllosilicates; Mars Science Laboratory; Gram-negative biomass; organic biosignatures

*Corresponding author. Email: rosalba.bonaccorsi-1@nasa.gov

ISSN 1478–6435 print/ISSN 1478–6443 online

DOI: 10.1080/14786435.2010.486374
http://www.informaworld.com

1. Introduction

One of NASA's key goals over the next several decades of planetary exploration is to determine whether life developed on planetary bodies in our solar system, including Mars. Mars is thought to have acquired the three key building blocks for life (water, an energy source, and a supply of organic molecules) in its geological history, but organic carbon has not yet been detected. The level one goal of the Mars Exploration Program Analysis Group (MEPAG) is the search for evidence of extinct or extant life (as we know it), and a complementary search for habitable zones for future missions.

The next decade of planetary missions, including the US 2011 Mars Science Laboratory (MSL11) and the ESA 2016 Pasteur ExoMars, will primarily seek key information on the geological and biological history of Mars. Clay minerals, or phyllosilicates, are unambiguously present on Mars. In analogy to Earth, phyllosilicate deposits on Mars have been recently suggested to support preservation of organic matter [1–4] and, as such, they have been selected as primary landing site candidates. In this context, a deeper understanding of preservation of biosignatures and habitability of phyllosilicate- and hematite/sulfate-rich analog materials can be achieved by studying new analog environments on Earth where these minerals are simultaneously present.

Performing habitability studies on heterogeneous environmental samples is certainly more complex and less reproducible than using synthetic minerals under controlled laboratory conditions. However, we believe that such complexity can be mitigated by an in depth knowledge of the environmental context (e.g. water availability, carbon/energy sources, potential microbiota sources). In addition, using complex mineral and astrobiology analogues for direct study of habitability potential would help unravel and interpret the true complexity arising from the investigation of a mostly unknown Martian environment.

In the first part of this paper, we present preliminary results from an ongoing, multidisciplinary investigation involving measurements of the total Gram-negative-like and total living microbial biomass (and the related organic biosignatures) as a relative proxy for habitability potential in dry and moist Mars-analog environments rich in clay minerals.

Specifically, we compared amounts of Gram-negative biomass in clay-rich (fine-grained) and non-clay (oxidized) materials to test whether or not phyllosilicates represent a preferential, and more habitable environment, for this class of microorganisms. Site and sample selection was based on four key criteria: (i) the simultaneous presence i.e. at stratigraphic/horizontal contact, of clay-rich and (ii) Fe-oxyhydroxides-rich/background materials; (iii) an easily verifiable source of organics and viable microbes common to both materials; and (iv) a well-known moisture gradient to explore the relationship between water availability and habitability of clays.

Phyllosilicate and hematite deposits under study are from a broad range of climates (hyper-arid, arid and semi-arid). Along the moisture gradient (<2 to $\sim$700 mm/year, rainfall, respectively) the Atacama Desert, Death Valley, and California Coast sites are diversely inhabited by life and have variable plant biomass and total organic carbon (TOC <0.1 to $\sim$3 wt%). Given the preliminary nature of

this work, clay minerals were identified from the bulk analysis of fine-grained samples. A well-detailed characterization of clay component (<2 μm) is planned for future work.

In the second part, a set of results from the microRaman Spectroscopy investigation on micrometer-sized particles, complemented with SEM/EDX (energy dispersive using X-ray), is provided for the same sample analyzed for Gram-negative biomass.

2. Background

2.1. *Phyllosilicate deposits and MSL11 landing site candidates*

Phyllosilicates, which record multiple episodes of aqueous activity on early Mars [1], have been identified on the surface of Mars by OMEGA, the visible-near infrared hyperspectral imager onboard Mars Express [5,6] and by the Spirit rover observation at West Spur, Columbia Hills, in Gusev Crater [7].

More recently, phyllosilicate-rich fluvial–lacustrine deposits e.g. in Eberswalde, Holden, and Jezero craters, as well as in the Nili Fossae region have been identified by the Mars Reconnaissance Orbiter (MRO) instruments, i.e. the high-resolution camera HiRISE and visible-infrared imaging spectrometer CRISM, e.g. [2]. More recently, CRISM observations have been used to identify stratigraphic units in Mawrth Vallis, comprising thick deposits of Fe/Mg-smectites, e.g. saponite, nontronite [1] ferrous phases, hydrated silica, and Al-smectites such as montmorillonite [2]. Furthermore, near-surface buried phyllosilicate deposits could exist on Mars [3,8].

Understanding the limit for organic preservation and habitability potential of these mineralogical analogues will provide critical information in support of landing site selection for the MSL11 and the EU/US Pasteur ExoMars Missions. All of the four MSL11 landing site candidates (http://marsoweb.nas.nasa.gov/landingsites/index.html) include clay deposits that have been hierarchically ranked by relevance with respect to context, diversity, habitability and preservation potential of organics in mineralogical/geological environments suggesting water activity [9]. Although habitability has been the most ambiguous criteria to be defined, it will be the most discriminating criteria for the final selection. MSL landing site selection is currently under consideration by the landing site Science Steering committee.

2.2. *Preservation of organics on Earth and Mars*

The search for organics on Mars is one of the primary objectives of the MSL Mission [10]. For instance, the instrument payload Sample Analysis at Mars (SAM) will include a pyrolysis–gas chromatograph–mass spectrometer (pyr-GC-MS) to detect a wide range of organic compounds in Martian materials [10,11,53]. Moreover, nucleobases and PAHs (polycyclic aromatic hydrocarbons) will be the target compounds for instruments as the Mars Organic Detector (MOD) payload of the ExoMars Mission.

The only information we have about organics on Mars derives from results of the Viking GC–MS experiments (and later by the Phoenix Mission). However, more recently, some have argued that the presence of organic carbon could have been

overlooked on Mars [12,13]. Meteoritic-delivered carbonaceous organic components on the surface of Mars [14,15] should be detectable in the Martian regolith in the absence of oxidative decomposition. It is expected that surface organics would not be preserved within the Martian regolith owing to oxidants production by physico-chemical interactions between solar UV radiation and the soil itself down to ~5-m depth [16–18]. Instead, buried organics may be well preserved in iron oxide-rich regolith against cosmic radiation [21]. However, in analogy with Earth, even buried organic biosignatures may be destroyed by metal-catalyzed oxidation within the Martian subsurface ([19] and references therein, [20]). Terrestrial organic matter is rarely preserved in oxidized minerals/oxidizing environments and this could be even truer for hematite sites associated with ancient wetlands on Mars, e.g. Meridiani Planum [4,19,22].

2.3. *Preservation potential of phyllosilicates*

A better model for the *in situ* search for organic compounds on Mars includes clay-rich deposits [4] owing to the ability of many clay minerals to promote formation [23] and sequestration of organics and inhibiting their decay. The long-term stabilization of dissolved organics absorbed on mineral surfaces [24–26] increases the mean residence time of organics in soils [29–30] and is likely the most effective protection against environmental oxidation [27,28].

The above mechanism seems to be effective also in mineral deposits. For instance, in the Rio Tinto (Spain) phyllosilicate-rich units [31] can preserve higher amounts of organic carbon than the embedding oxidized rocks [4]. Further explanation is given in Figure 1.

3. Study areas

3.1. *Hyper-arid Atacama Desert*

Phyllosilicate-rich deposits (Figures 2a and b, light toned) and hematite-rich brines (dark toned in Figures 2a and b) were newly observed and sampled in the hyper arid core of the Atacama Desert near Yungay (Antofagasta region, Chile). The Atacama Desert represents the driest, and most life-depleted, place on Earth [48–50]. Coarse-grained Atacama soils are typically alluvial containing particles of primarily granitic (quartz, feldspars) and mafic (basalts) origin concentrated in the gravel- to silt-sized fraction; gypsic horizons are present below 2–3 cm depth [60]. Low amounts of clays (smectite, chlorite and kaolinite, fraction 0.2–2.0 μm) can be present at the surface and at some depth [60,61]. These soils are characterized by very low levels of refractory organics (at the 0.01 %wt.) at the hyper-arid extreme [49], while both biomass and preserved organics typically increase with density of vegetation cover along a latitudinal/altitudinal rainfall gradient [39,49,50].

3.2. *Arid Death Valley*

Little Hebe is a young (300 year) and small spatter cone (formed by molten lava) located in the Ubehebe volcanic field in the Death Valley National Park,

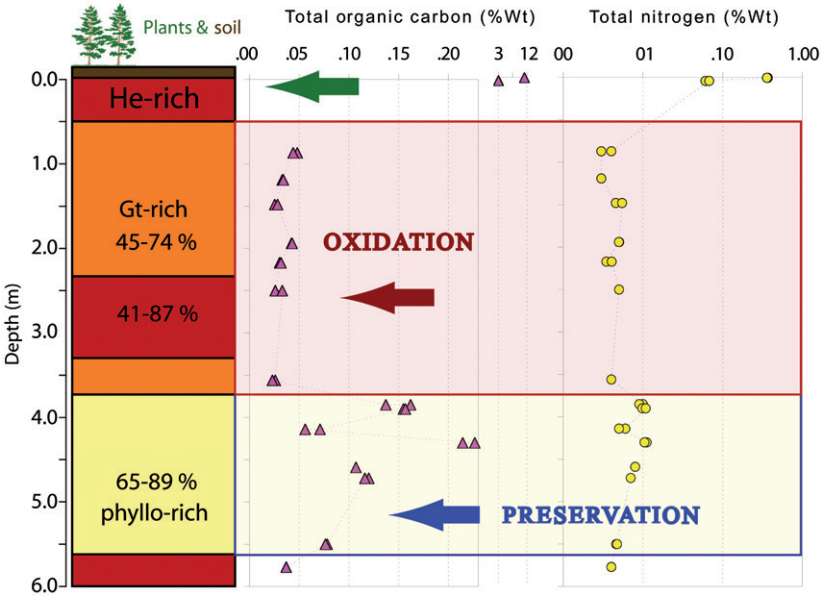

Figure 1. Conceptual oxidation/preservation model from the Rio Tinto analog; after [4]. The dissolved organic carbon (DOC) of this pine forest soil is entrained by rain (500–700 mm/year) and can be absorbed, and "rapidly" oxidized, or preserved within shallow materials. Shallow near-surface phyllosilicate-rich zones, e.g. muscovite–illite, kaolinite, and smectite (montmorillonite), preserve up to ten-times more organic carbon (OC: ~0.23 wt% blue arrow) than the embedding hematite-(He) and goethite (Gt)-rich rocks (OC: <0.04 wt% red arrow). Organic carbon was surprisingly low (<0.04 wt%), even just a few cm beneath the organic-rich "O" Horizon (OC: 3–12 wt%, green arrow).

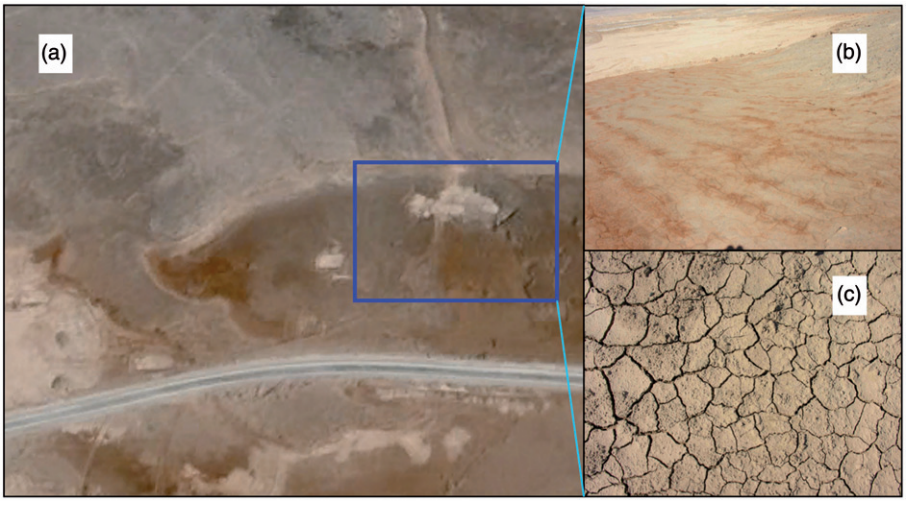

Figure 2. Atacama Desert. Landscape view of contiguous oxidized brine- and clay-rich deposits (a) enlarged to show meter-scale banded structures alternating dark-toned (non-clay) and light-toned (clays) deposits (b) exhibiting a polygonal structure (c).

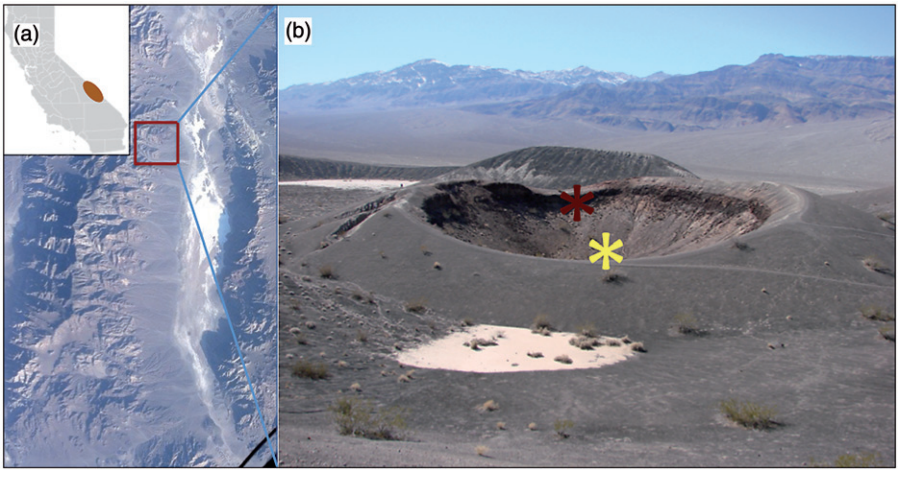

Figure 3. (Color online). Location of Death Valley National Park with inset for the Hubehebe Field (a). Little Hebe Crater (b). Sample locations are indicated by the top (red online) (crater rim) and bottom (yellow online) (crater bottom) asterisks. Crater bottom is not visible here. Figure 3a credit: STS073-E-5119: NASA JSC.

California (Figure 3a). The whole field comprises over 13 maar volcanoes formed by subsequent phreatomagmatic explosions (late Holocene) exposing conglomerate Miocene deposits [32]. The area is sparsely colonized by plants, e.g. Desert Holly (*Atriplex hymenelytra*), Creosote bush (*Larrea tridentata*), and comprises alluvial/aeolian fine-grained deposits (Figure 3b).

Samples of dry surface materials were taken from the Little Hebe crater (Figure 3b). The hematite-rich gypsum-bearing sample (HUBE08-3D) is from an oxidized cemented sandstone outcrop in the crater rim (red symbol), which is plant-barren, and relatively dry from exposure to frequent strong winds. The silty-clay sample (HUBE08-3C) was taken from a light-toned pond deposit at the crater bottom (yellow symbol).

3.3. *Moist California Coast*

Pescadero State Beach is located in the coastal region of California (Figure 4a), which is characterized by a semi-arid Mediterranean climate (700 mm/year rainfall), low fog and overcast year round. This site represents the moister and more habitable end-member.

Samples were taken from an exposed outcrop (Figures 4b and c) comprising water-saturated estuarine mud, predominantly gray and blue clay [51], capped by an oxidized, goethite-rich, poorly consolidated sandstone level (Figure 4c). Soil atop these units (Figure 4b) is extensively colonized by cordgrass (*Spartina* sp.), and pickleweed (*Salicornia* sp.).

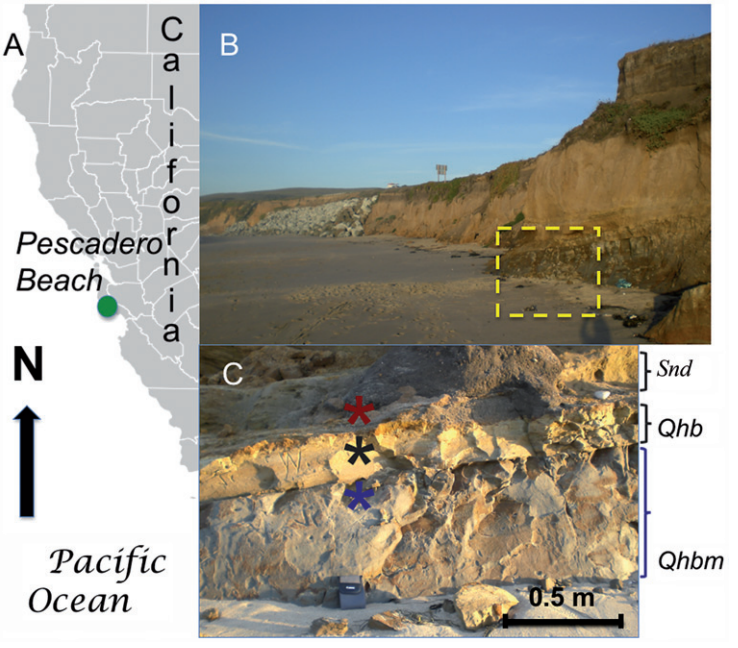

Figure 4. Location (a), general setting (b) and stratigraphy (c) of exposed outcrops sampled (asterisks) at Pescadero State Beach. Bottom to top in (c): (i) "blue clays" or Qhbm (Holocene bay mud); (ii) "gray clays" or Qhb (Holocene basin deposit) [51]; and (iii) overlying sandstone level (Snd).

4. Approach and methods

We use the term "clay" for fine-grained material (silty-clay and clay-sized) exhibiting strongly cohesive and plastic characteristics upon wetting and handling [62]. Sample texture and water content (weight % of water in a given mass) were determined by using standard procedures [63]. The clay mineral composition of three fine-grained samples was subsequently characterized with XRD analysis.

We analyzed clay-rich against non-clay materials in order to determine their habitability potential and the effect of increasing environmental moisture on living biomass inhabiting clay-rich deposits. Overall, we used field assays for the detection of unequivocal biological markers as proxies for total living and Gram-negative biomass.

4.1. *Total Gram-negative biomass*

The LPS-based, or Gram-negative biomass in the rock and mineral samples was determined with a portable system (Charles River Laboratories PTS System Package 550®) based on the Limulus amebocyte lysate assay, or LAL [33]. This is an extremely sensitive non culture-based method to measure, in a relatively rapid and accurate manner, the amount of lipopolysaccarides, or LPS (aka the microbial endotoxin) in the environment. LPS are present in the external cellular membrane of

a wide range of Gram-negative-like microorganisms, including cyanobacteria [34], unicellular algae [35], green algae and even selected vascular plants, i.e. eukaryote chloroplasts [36].

A triple water extraction was performed on 1 g of well-homogenized mineral and soil samples. For each extraction, 2 ml of high-quality ultrapure water (Milli-Q® Advantage A10) was added to samples in 15 ml sterile falcon tubes. These were vortexed (20 s), sonicated (40 s) and centrifuged at high speed for 5–10 min as per NASA Procedural Requirements [37]. Then, 50–100 µl of clear supernatant was diluted 10–1000 times with ultrapure pyrogenic free-water (LAL reagent water), vortexed for 1 min and immediately assayed together with the appropriate negative control. Finally, four 25-µl aliquots of this solution (a duplicate sample, and a duplicate spiked sample as positive control) were loaded on single-use cartridges as per manufacturer's direction. Basically, in the LAL assay the bacterial endotoxin released from samples catalyzes activation of a proenzyme triggering a colorimetric variation (change in color) that is measured by the spectrophotometer (405–410 nm). This yields a value expressed in endotoxin units (EU/ml) that can be directly converted into total Gram-negative microbial biomass (cell/g); 1 EU/ml is equivalent to $\sim 10^5$ cells/ml (*E. coli*-like cells).

This assay has been routinely used to detect endotoxin contamination in environmental liquid samples and biopharmaceutical products. More recent applications include Planetary Protection protocols [37], and astrobiology investigations [54,55].

4.2. *Total viable biomass*

The portable hygiene monitoring system LIGHTING MVP (BioControl Systems, Inc., WA, USA) was used to assay levels of adenosine 5′-triphosphate (ATP). As the ATP is the energy system carrier used by all living organisms, this technique can be applied to estimate the metabolically active cells, or total viable biomass in soil samples [38]. Soil and mineral particles were dispersed onto a standard surface area ($\sim 9\,cm^2$), swabbed uniformly (5 min swabbing time), and assayed with surface sampling devices. The ATP activity is expressed as relative luminosity units (RLUs) and reflects the total viable biomass in a sample. The ATP-based biomass values can be then calibrated versus phospholipids fatty acid (PLFA)-based total biomass (cell/g soil) on sub aliquots of primary soil samples tested for ATP [39]. Details on methods are described in full elsewhere (see [4,40], and references therein]).

4.3. *X-ray diffraction*

Sample bulk mineralogy (53-µm size fraction) was assessed at the Evans Analytical Group (EAG, Sunnyvale, CA). Samples were crushed to pass through a 53-µm sieve, back loaded to minimize preferred orientation effects with a Rigaku Ultima III diffractometer in standard θ:2θ coupled geometry with Cu radiation, variable slits and a diffracted beam monochromator. The relative amount of clay component in the fine-grained samples was estimated by comparing the peak at about 19.7° (2θ) or 35° (2θ), representing several clay minerals such as kaolinite, illite, and smectites, with the peak at about 20.8° (2θ) relative to quartz.

4.4. *MicroRaman spectroscopy*

We used conventional microRaman spectroscopy to detect organic biosignatures in complex geological samples [41], complemented by mineral phase identification, geochemical and microbiological assays. Unprocessed samples were analyzed with a dispersive microRaman/photoluminescence spectrometer (Renishaw InVia) at the NASA Ames Advanced Science Laboratories (ASL) facility.

Spectra from Sample HUBE08-2D were acquired with 5×, 20× and 50× microscope objectives from three lasers i.e. 514, 633 and 785 nm excitations, that enable the collection of spectral signatures of about 2 μm diameter and a theoretical confocal depth of about 2 μm. Raman spectroscopy is based on inelastic photon scattering by molecules, in which the wavelength of the scattered photon differs from that of the incident photon. Raman scattering is most sensitive to chemical bounds C–C, C–N, C=C, C=O, S–S C–N and P–O, which have Raman lines between 1100 and 1800 cm^{-1} in organic and biogenic organic molecules. Microbial cells contain carbohydrates, lipids, proteins, and nucleic acids with distinct Raman spectra, e.g. 750–1110 cm^{-1} [47]. The Raman spectroscopy has been used successfully for the *in situ* detection of individual bacteria and other microorganisms [42,43], complex biomolecules, and to determine the biogenic [44] versus non-biogenic nature [45,46] of putative-like microfossils.

5. Results and discussion

5.1. *Mineralogical compositions of fine-grained samples*

Diffractograms for three out of eleven samples are shown in Figure 5. Samples contain different phyllosilicates assemblages as well as non-clay phases characterized by a different degree of complexity for XRD-based identification. For general identification of non-clay mineral phases, the best matches versus the International Centre for Diffraction Data (ICDD/ICDS) database are overlaid on the experimental data.

For the three samples the following mineralogical interpretation can be inferred from XRD patterns presented in Figure 5.

Overall, from the relative peak intensity at about 19.7° (2θ) or 35° (2θ), Sample AT08-YU-42C, YU seems to contain a higher amount of clay minerals than Sample HUBE08-3C, which in turn is richer than Sample PES08-1B.

Figure 5.1 shows data for sample AT08YU-42C taken from desiccation polygons (Figures 2b and c) at a novel site in the Atacama Desert (Figure 2). Overall, this sample contains smectites, probably a Ca-montmorillonite (wide peak at about 6°), mixed layer illite/smectites (I/S) (wide band in the range 6–9°), illite or muscovite (peak at 8.9°), and chlorite + kaolinite (peak at about 12.4°). While this sample is also high in quartz, it seems to contain more potassium-bearing minerals (microcline and albite) than the other samples, as well as calcite (peak at 29.4°). Moreover, the presence of gypsum could be consistent with a faint peak at about 11.5°.

Figure 5.2 shows data for sample HUBE08-3C collected from the Little Hebe area (Figure 3). This pattern is very complex and phase identification is difficult. This sample contains smectites, probably Ca-montmorillonite (wide peak at about 6°),

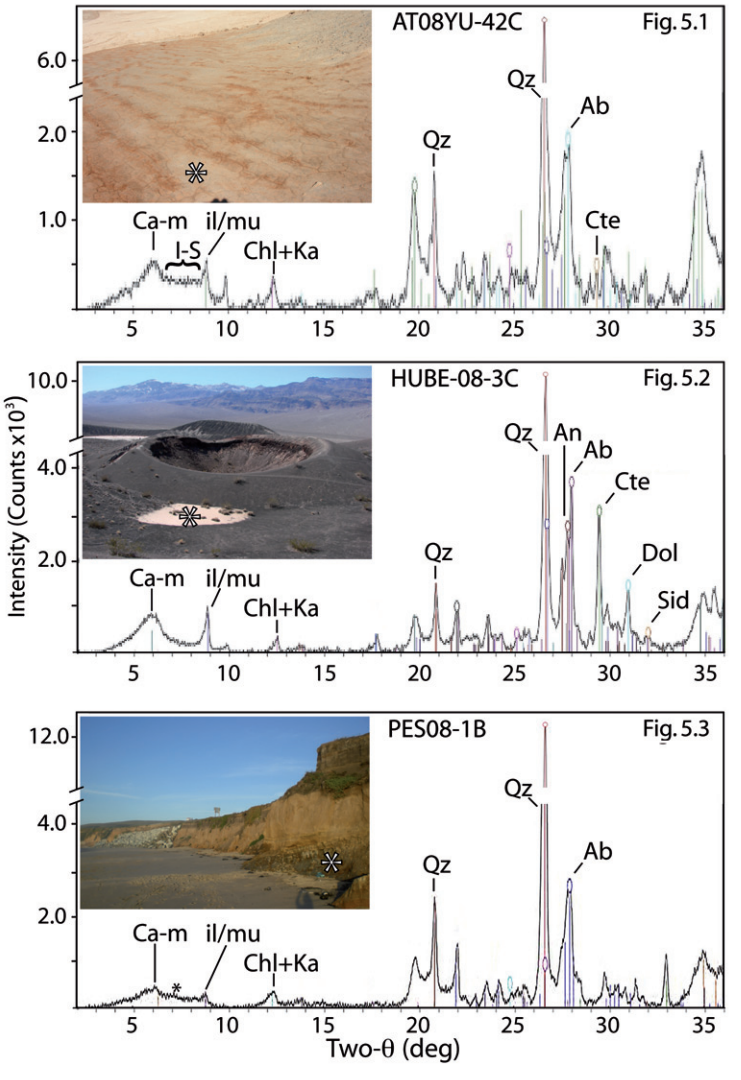

Figure 5. (Color online). Diffractograms (background subtracted raw data) for samples from the Atacama Desert (5.1), Little Hebe crater (5.2), and Holocene blue clay unit (5.3). Asterisks show sampling sites. Illite/smectites mixed layer (I-S); illite (ill); chlorite (chl); kaolinite (ka); Ca-montmorillonite (ca-m); muscovite (mu); quartz (Qz); albite (Ab); anortite (An); calcite (ctc); dolomite (Dol); and siderite (Sid).

illite or muscovite (peak at 8.9°), chlorite + kaolinite (peak at about 12.4°), quartz, un-weathered silicates (plagioclase such as albite and anortite), and some carbonates (calcite, dolomite, and siderite). The XRD also shows a faint peak at about 9.8° to be identified. Sample HUBE08-3C seems to have a more diverse content, in agreement with plausible multiple sources (wind-blown, fluvial) from exposed parent materials, i.e. Holocene acid volcanic tuffs and Miocene alluvial deposits [32].

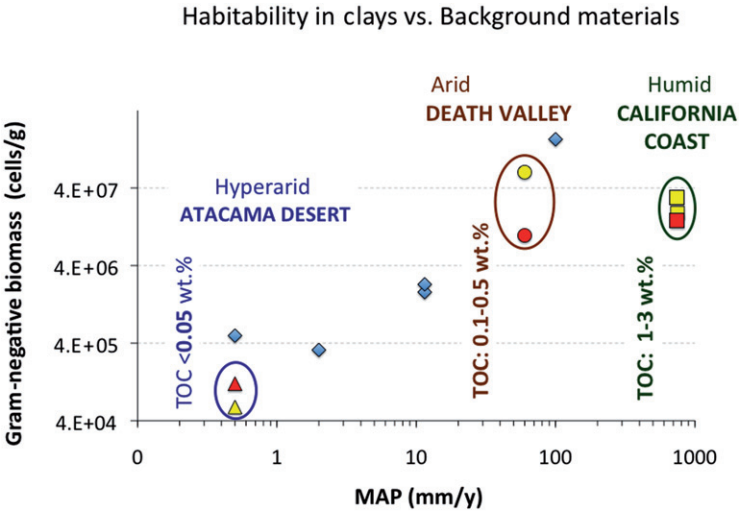

Figure 6. Biomass concentrations of phyllosilicate- (light-toned symbols) versus Fe-oxide-rich samples (dark-toned) along the rainfall gradient. Left to right: samples from (1) the Atacama (triangles), (2) Death Valley (dots), and Pescadero (squares) sites. Diamond-shaped symbols indicate coarse-grained, non-clay soils (Table 1). Error bars for sample CV% < 25 ($N = 2$) are inside the marks. For explanation see the main text. Organic content information (TOC, wt%) for the three sites is based on literature data [39,64].

Finally, Figure 5.3 shows phases in the coastal Sample PES08-1B (Figure 4) that was simpler to determine with respect to the two above. It contains smectites, probably Ca-montmorillonite (wide peak at about 6°), possibly mixed layer illite/smectites (I/S) (smooth wide band in the range 6–9°), illite or muscovite (peak at 8.9°), chlorite + kaolinite (peak at about 12.4°), quartz, and plagioclase (albite).

Phyllosilicate phases in these samples appeared to be similar to those identified, or inferred to exist on the Martian surface [2,5–7]. However, these results are preliminary and qualitative.

Specifically, phyllosilicate phase identification on the bulk fraction (<53 μm) is difficult owing to the presence of several mineral phases and mixed-layer phyllosilicates. A detailed analysis of the <2-μm size fraction on preferentially oriented specimens will be required for the complete quantitative and qualitative characterization of phyllosilicates in these mineralogical Mars analogs.

5.2. *Viable biomass in mineral environments*

We successfully applied the LAL assay to determine the LPS-based, or Gram-negative-like biomass in rocks and fine-grained materials. All values of endotoxin recovery were within the acceptable ranges, i.e. 50–200% of spike recovery, and sample CV% < 25. Gram-negative biomass in clay vs. non-clay materials is reported in Figure 6 and plotted against the mean annual precipitation (MAP) gradient. Additional information is given in Table 1.

Table 1. Synoptic information for samples analyzed in this study. Viable biomass data are given for fine grained and coarse-grained materials (Figure 6). Gram-negative biomass data obtained with the LAL assays. Results of the ATP assay refer to the ATP activity reported with the main statistic; only the highest RLU values and the standard deviations for three replicates are showed. EU: endotoxin units; RLU: relative luminosity units. NA: not analyzed/under analysis.

Sample name	MAP (mm/y)	Location	Depth (cm)	Type	Water content (wt %)	LPS EU/mL (N = 2)	Sample CV%	Spike recovery	Gram (-) biomass cells/g	ATP assay RLUs Avg ± STDEV	Texture and description
AT08-11, 0-2	**100**	*Atacama, La Serena*	0-2	SOIL	15.4 ± 1.3	334	7.4	94	1.7×10^8	NA	Coarse-grained hematite-rich, sandy silt top soil (20% plant cover).
AT06-03, 0-1	**11.5**	*Atacama, Copiapo'*	0-1	SOIL	2.6 ± 0.6	3.47	5.5	88	1.8×10^6	21573 ± 812	Light gray silty-sand. Plant-barren
AT06-05, 0-3	**2**	*Atacama, Taltal*	0-3	SOIL	2.2 ± 0.7	0.55	0.6	100	3.3×10^5	388 ± 35	Light brown silty sand. Plant-barren
AT08-ANT-25	**0.5**		0-2	SOIL	0.87 ± 0.93	<1.01	0.0	90	$<5.0 \times 10^5$	NA	Light brown sandy silt (coarse sand). Plant-barren
AT08-YU-42C	**0.5**	*Atacama, Yungay*	0-3	CLAY-RICH	1.2 ± 0.7	< 0.10	0.0	109	$<5.0 \times 10^4$	NA	Light yellow silty clay. Plant-barren
AT08-YU-42B	**0.5**		0-2	FE-OXIDES	3.2 ± 1.2	< 0.20	0.0	85	$<1.2 \times 10^5$	NA	Reddish brown silty sand deposit. Hematite-rich w/salts
HUBE08-3C	**60**	*Little Hebe crater (DVNP)*	0-1	CLAY-RICH	7.8 ± 0.5	106	20.2	107	6.4×10^7	NA	Light yellow clayey silt deposit (10% plant cover)
HUBE08-3D	**60**		0-2	FE-OXIDES	2.3 ± 1.8	15	15.5	205	9.8×10^6	NA	Dusky red, hematite-/ gypsum-rich sandstone/ basalt scoria. Plant-barren
PES08-2C	**750**		(*)	FE-OXIDES	15.4 ± 2.9	31.4	11.3	201	1.9×10^7	2858 ± 1461	Goethite-rich oxidized sandstone (100% Plant cover)
PES08-2D	**750**	*Pescadero State Beach*	(*)	CLAY-RICH	59.6 ± 1.4	24.1	5.8	92	1.5×10^7	912 ± 200	Gray mud (silty clay); water-saturated estuarine mud
PES08-1B	**750**		(*)	CLAY-RICH	57.6 ± 2.9	48.8	4.7	207	3.0×10^7	1475 ± 514	Dark olive gray mud (clayey silt) water-saturated estuarine "blue mud"

Note: Asterisks indicate surface samples (c.f. Figure 4).

5.2.1. *Atacama Desert*

Clays from desiccation polygons (Sample AT08YU-42C) contain smectites, illite-muscovite and chlorite + kaolinite phases and represent the extreme hyper-arid end-member used in this study. The viable biomass content ($\sim 6.0 \times 10^4$ cells/g, yellow triangle) of these fine-grained deposits is similar to that of contiguous hematite- and salts-rich one (Sample AT08YU-42B: red triangle; $\sim 1.2 \times 10^5$ cells/g). When compared with coarse-grained soils from this region (Samples AT08-ANT-24 and AT06-05: $3.3–5.0 \times 10^5$ cells/g; Figure 6, blue diamonds), both phyllosilicate- and hematite-/salts-rich deposits contain the lowest biomass.

5.2.2. *Ubehebe Crater Field*

The silty-clay Sample HUBE08-3C (smectites, illite–muscovite, and chlorite + kaolinite) yielded higher biomass ($\sim 6.4 \times 10^7$ cells/g) than the hematite-/gypsum-rich sample ($\sim 9.8 \times 10^6$ cells/g) from the crater rim (HUBE08-3D). Difference between these two samples could be explained by the likely presence of plant-associated, *in situ* microbial biomass and/or inputs of wind blown microbes to the silty-clay pond deposits, and colonization of gypsum grains by cyanobacteria (Section 5.3).

5.2.3. *Pescadero State Beach*

Overall, no relevant difference exists between the Gram-negative biomass in the two types of mud and the overlying oxidized porous sandstone (Figure 6). The clay-rich units and the oxidized sandstone level (Sample PES08-2C) contain similar amounts of biomass ($1.5–3.0 \times 10^7$ cells/g) and exhibit similar ATP activity i.e. 1475 ± 514, 912 ± 200 and 2858 ± 1461 RLUs, respectively. The blue clay Sample PES08-1B (smectites, illite-muscovite, and chlorite + kaolinite) also bears a slightly higher level of living biomass than the overlying gray mud unit (Sample PES08-2D). Gram-negative-like organisms inhabiting these exposed units could have multiple provenances. Soil atop the cliff deposits is extensively covered (100%) with cordgrass (*Spartina* sp.) and pickleweed (*Salicornia* sp.) (Figure 4). In addition to horizontal fluxes of biomass thru coastal fog, and ocean spray, both clay and non-clay materials can be colonized by microrganisms from the near-surface soil horizons.

When comparing living biomass content of clay and non-clay (oxidized) background materials from the three locations described above, no definitive conclusion can be made on whether or not clay mineral-rich environments have a higher habitability potential with respect to that of background materials.

5.2.4. *Viable biomass of fine-grained materials versus moisture gradient*

Figure 6 shows that there is a significant difference in viable Gram-negative biomass of silty-clay and clay-sized samples between the hyper-arid (MAP < 2 mm/year) and arid (>10 to <100 mm/year) sites. More specifically, biomass in Sample AT08-YU-42C from the hyper-arid Atacama region resulted three orders of magnitude lower than in Sample HUBE08-3C from the arid Death Valley, i.e. $\sim 6.4 \times 10^7$ cells/g, <10 wt% water content. The latter represents a biomass level up to six-times higher than that found in wet clays (~ 60 wt%, with $1.5–3.0 \times 10^7$ cells/g) from the ten-times

moister coastal site, i.e. >700 mm/year (Figure 6, right-hand side). This result is apparently counterintuitive. Clay-rich units from the coastal site are expected to contain a higher and likely most diverse biomass (terrestrial and marine) with respect to the desert locations. Rather, these preliminary results suggest that, in these fine-grained sediments the increasing moisture content does not always result in higher biomass, and that wet silty-clay/clay materials might be even less habitable than dry clay-rich ones.

Typically, total and Gram-negative biomass of coarse-grained (non-clay) soil linearly increases along the rainfall gradient such as at the arid/hyper-arid transition in the Atacama Desert [13,39,50]. This relationship has been confirmed by our new dataset (solid diamond symbols) but may not apply to clay-rich materials from arid to moist environments (Figure 6).

Levels of living biomass inhabiting fine-grained deposits could be related not only to the potential sources of organics and biomass in the surrounding environment, but also to the interplay of several factors, including but not limited to, amount and type of clay mineral phases, bulk material grain size and porosity, as well as variable moisture (precipitations, fog) influencing the degree of clay wetting year round.

The current definition of habitability is linked with the availability of liquid water [2,5,6,9,10]. Clays are generally considered protective and habitable environments for various microorganisms. However, water-saturated clay mineral-rich materials may represent a challenging, hostile environment for microbes. For instance, some clay minerals (e.g. smectites) upon wetting can exhibit definitive antibacterial action as a result of their physicochemical properties [56,57]. Mechanisms could involve physical [58] and metabolic disruption (e.g. by affecting permeability of cell outer membranes), and/or cell suffocation by precipitation of a solid phase onto cells; additional factors may include poisoning by released toxins, and impeded nourishment in nutrient-limited environments [59].

5.3. *Raman spectroscopy investigations*

Results of the multi-component investigation conducted on the sample from the Little Hebe crater rim are shown in Figure 7. Overall, we were able to simultaneously capture mineralogical and possibly biological features by using a microRaman spectroscopy tool. The sample in question is dominated by hematite [Fe_2O_3] and gypsum [$CaSO_4 \cdot 2H_2O$] minerals and is associated with the 1281 cm^{-1} spectral band assigned to the scytonemin pigment signature associated with cyanobacteria [52]. The multi-wavelength Raman spectrometer instrument, e.g. 514, 633 and 785 nm excitation based on a confocal sampling arrangement, enables extraction of spectral data from a complex system such as cyanobacteria/gypsum substrates [52]. Gypsum matrix spectra can exhibit bands at 1142, 1008, 618, 493, 414, 211 and 181 cm^{-1} (at 785 nm) [52]. Cyanobacterial colonies exhibit signature bands at 1630, 1598, 1552, 1454, 1379 and 1281 cm^{-1} (Figure 7c) assigned to the scytonemin pigment, while signature at 1330 cm^{-1} is assigned to chlorophyll (see [52] and references therein). In the study case, the microRaman spectra signatures indicative of gypsum and hematite minerals as well as proxy biomarkers for cyanobacteria were consistent

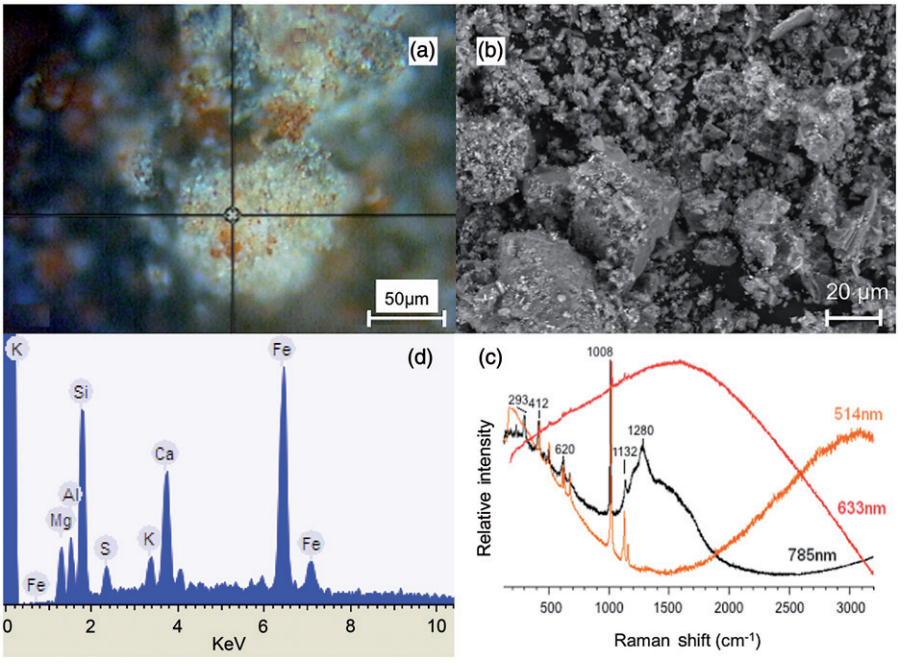

Figure 7. Distinct microRaman spectra signatures of sample from the Little Hebe crater rim (b) simultaneously showing mineralogical and microbiological spectral signatures of gypsum at 1008, 620, 493 and 211cm^{-1} (at 785 nm) and hematite at 293, 412, 498 and 660 cm^{-1}. Cyanobacterial colonies band at 1280 cm^{-1} is assigned to the scytonemin pigment (at 785 nm). The assignments are supported by compositional EDX spectra (d), optical (a, 20 × microscope objective), and SEM observations (b).

with, and complemented by (a) the optical identification of gypsum aggregates (Figure 7a); (b) the visual identification of hematite; (c) the presence of Ca, S, and Fe (Figure 7d), and (d) our independent measurement of Gram negative-like organisms, i.e. $\sim 10^7$ cell/g (Section 5.2.2 and Figure 6).

A microRaman instrument is included in the ExoMars payload, which will also perform studies on phyllosilicates. Data generated from direct analysis of environmental samples will be critical to verify the applicability of Raman spectroscopy and the search for proxies for past and present life in phyllosilicate deposits.

6. Conclusions

6.1. *LAL assay*

We quantified the amount of the LPS biomarker as a rapid and sensitive way to determine the Gram-negative biomass. This is a rather novel and successful approach to explore the preservation of organic biosignatures and habitability potential in fine-grained materials.

6.2. *XRD analysis*

A detailed analysis of XRD patterns has shown that the clay mineral component is higher in the hyper-arid Atacama site than in the arid Death Valley and moister coastal sites. However, from this preliminary study, it is uncertain whether the living biomass amount is correlated to the abundance and type of clay mineral components.

6.3. *Phyllosilicate versus iron-rich minerals*

When comparing biomass in clay-rich vs. non-clay materials, we can distinguish three contrasting cases: (i) the newly observed Atacama polygonal clay blocks contain about the same viable biomass than the coexisting hematite-rich materials. This is the lowest biomass ($\sim 10^4$ cells/g) against that of coarse-grained, clay-poor, soil ($\sim 10^5$ to $\sim 10^6$ cells/g) extensively known from the literature; (ii) the clay-bearing deposit from Death Valley (~8 wt% water content) contains significantly more Gram-negative biomass ($\sim 10^7$ cells/g) than the hematite/gypsum-rich sample ($\sim 10^6$ cells/g); and (iii) there is no significant difference between clay-rich and goethite-rich units exposed at Pescadero State Beach.

From these preliminary results it is unclear whether or not clay mineral-rich environments have a higher habitability potential with respect to that of background, clay mineral-barren/coarse-grained soil environments. Therefore, a wider number of study sites should be tested to determine the effective role of minerals in hosting viable biomass.

6.4. *Fine-grained materials versus rainfall gradient*

There is an overall significant difference between biomass content of samples from the hyper-arid Atacama and the arid Death Valley. However, and unexpectedly, fine-grained dry materials from the Death Valley contain up to six-times more biomass than water-saturated mud (~60 wt%) from the ten-times moister coastal site (Figure 4). This last result is counterintuitive and seems to imply that, at least for this study case, fine-grained deposits from an arid environment might be more habitable than those from a moist environment. Apparently, in these wet mud deposits increasing vegetation cover and year round moisture did not translate into a higher content of living biomass. Factors such as grain size, porosity, type and abundance of clay minerals, as well as variable water contents could be responsible for the differences encountered. For instance, physicochemistry of wet clays (increased ionic exchanges) may control mechanisms for inhibiting microbial growth/survival in clay-dominated moist environments.

6.5. *MicroRaman investigations*

At least for the studied case both mineralogical and biological features, consistently with literature data, were successfully captured and validated by complementary measurement on the same sample analyzed for living biomass.

6.6. *Future studies*

We plan to perform an in-depth study of clay mineralogy on the <2-μm size fraction of fine-grained deposits as Mars analog environments. A quantitative characterization of the occurring clay minerals, indeed, could help us to understand the role of physicochemical factors (water availability, ionic exchanges, water absorption capacity) as controlling mechanisms of microbial growth/survival in phyllosilicate-dominated environments.

A deeper understanding of habitability of phyllosilicate- and hematite-rich materials, achieved by studying new analog sites where these minerals occur simultaneously, will provide critical information to help identify the best locations to search for recent and ancient organic biosignatures on Mars and in support of data returned from the next decade missions.

Acknowledgements

We thank Stephen B. Robie (EAG), John Noble for graphics development and Carrie Chavez for editorial assistance. We also thank an *anonymous referee* for helpful comments and assistance with interpretation of clay minerals data. This research has been partially funded by the NASA Planetary Protection Program.

References

[1] B.L. Ehlmann, J.F. Mustard, C.I. Fassett, S.C. Schon, J. Head III, D.J. Des Marais, J.A. Grant and S.L. Murchie, Nature Geosci. 1 (2008) p.355.
[2] J.L. Bishop, E.Z. Noe Dobrea, N.K. McKeown, M. Parente, B.L. Ehlmann, J.R. Michalski, R.E. Milliken, F. Poulet, G.A. Swayze, J.F. Mustard, S.L. Murchie and J.P. Bibring, Mars Sci. 321 (2008) p.830.
[3] V. Chevrier, Nature Geosci. 1 (2008) p.348.
[4] R. Bonaccorsi and C.R. Stoker, Astrobiology, 8 (2008) p.967.
[5] F. Poulet, J.-P. Bibring, J.F. Mustard, A. Gendrin, N. Mangold, Y. Langevin, R. Arvidson, B. Gondet, C. Gomez and the Omega Team, Nature 438 (2005) p.623.
[6] J.-P. Bibring, V. Langevin, J.F. Mustard, F. Poulet, R. Arvidson, A. Gendrin, B. Gondet, N. Mangold, P. Pinet, F. Forget and the Omega Team, Science 312 (2006) p.400.
[7] A. Wang, R.L. Korotev, B.L. Jolliff, L.A. Haskin, L. Crumpler, W.H. Farrand, K.E. Herkenhoff, P. de Souza Jr., G.A. Kusak, J.A. Hurowitz and N.J. Tosca, J. Geophys. Res. 111 (2006) p.E02S16.
[8] D.C. Catling, Nature 448 (2007) p.31.
[9] L. Beegle, M. Wilson, F. Abilleira, J. Jordan and G. Wilson, Astrobiology 7 (2007) p.4.
[10] P. Mahaffy, Space Sci. Rev. 135 (2008) p.255.
[11] D.P. Glavin, H.J. Cleaves, A. Buch, M. Schubert, A. Aubrey, J.L. Bada and P. Mahaffy, Planet. Space Sci. 54 (2006) p.1584.
[12] H.P. Klein, J. Orig. Life Evol. Biospheres 21 (1992) p.1573.
[13] R. Navarro-González, K.F. Navarro, J. de la Rosa, E. Iñiguez, P. Molina, D. Luis, L.D. Miranda, P. Morales, E. Cienfuegos, P. Coll, F. Raulin, R. Amils and C.P. McKay, Proc. Natl. Acad. Sci. USA. 103 (2006) p.16089.
[14] W. Van der Velden and A.W. Schwartz, Geochim. Cosmochim. Acta 41 (1977) p.961.
[15] P.G. Stoks and A.W. Schwartz, Nature 282 (1979) p.709.
[16] M.A. Bullock, C.R. Stoker, C.P. McKay and A.P. Zent, Icarus 107 (1994) p.142.

[17] A.P. Zent, J. Geophys. Res. 103 (1998) p.31491.
[18] H. Lammer, H.I.M. Lichtenegger, C. Kolb, I. Ribas, E.F. Guinan, R. Abart and S.J. Bauer, Icarus 165 (2003) p.9.
[19] D.Y. Sumner, J. Geophys. Res. 109 (2004) p.E12007, doi:10.1029/2004JE002321.
[20] R. Apak, Int. J. Astrobiol. 7 (2008) p.187.
[21] A. Aubrey, H.J. Cleaves, J.H. Chalmers, A.M. Skelley, R.A. Mathies, F.J. Grunthaner, P. Ehrenfreund and J.L. Bada, Geology 34 (2006) p.357.
[22] A.F. Davila, A.G. Fairén, L.G. Duport, C.R. Stoker, R. Amils, R. Bonaccorsi, J. Zavaleta, D. Lim, D. Schulze-Makuch and C.P. McKay, EPSL 272 (2008) p.456.
[23] G. Ertem, R.M. Hazen and J.P. Dworkin, Astrobiology 7 (2007) p.715.
[24] L.P. D'Acqui, E. Daniele, F. Fornasier, L. Radaelli and G.G. Ristorri, Eur. J. Soil Sci. 49 (1998) p.579.
[25] K. Kaiser and W. Zech, J. Plant Nutr. Soil Sci. 163 (2000) p.531.
[26] M. Kleber, R. Mikutta, M.S. Torn and R. Jahn, Eur. J. Soil Sci. 56 (2005) p.717.
[27] J.I. Hedges and R.G. Keil, Mar. Chem., 49 (1995) p.81.
[28] G.L. Cowie, J.I. Hedges, F.G. Prahl and G.J. De Lange, Geochim. Cosmochim. Acta 59 (1995) p.33.
[29] M.S. Torn, S.E. Trumbore, O.A. Chadwick, P.M. Vitousek and D.M. Hendricks, Nature 389 (1997) pp.170–173.
[30] E.J.W. Wattel-Koekkoek and P. Buurman, Soil Sci. Soc. Am. J. 68 (2004) p.154.
[31] B. Sutter, A.J. Brown and C.R. Stoker, Astrobiology 8 (2008) p.1049.
[32] B.M. Crowe and R.V. Fisher, Geol. Soc. Am. Bull 84 (1973) p.663.
[33] J. Bruckner and K. Venkateswaran, Jpn. J. Food Microbiol. 24 (2007) p.61.
[34] C.R.H. Raetz and C. Whitfield, Annu. Rev. Biochem. 71 (2002) p.635.
[35] J.C. Bedick, A. Shnyra, D.W. Stanley and R.L. Pardy, Naturwissenschaften 88 (2001) p.482.
[36] M.T. Armstrong, S.M. Theg, N. Braun, N. Wainwright, R.L. Pardy and P.B. Armstrong, FASEB J. 20 (2006) p.2145.
[37] NASA Procedural Requirements, NPR 5340, 2007.
[38] D.A. Cowan, N.J. Russell, A. Mamais and D.M. Sheppard, Extremophiles 6 (2002) p.431.
[39] R. Bonaccorsi and C.P. McKay, *Total biomass and organic carbon along a N-S moisture gradient of the Atacama region, Chile* [abstract 1489], in *39th Lunar and Planetary Science. Conference Abstracts*, Lunar and Planetary Institute, Houston, TX, 2008.
[40] D.P. Miller, R. Bonaccorsi and K. Davis, Astrobiology 8 (2008) p.947.
[41] B. Chen, N. Cabrol, C.R. Stoker, C.P. McKay, R. Bonaccorsi, J. Zavaleta, S. Dunagan, J.A. Rodriguez-Manfredi, J. Gomez Elvira and F. Rul (eds.). Raman spectra identifications of mineral and organic constituents. NASA Science Technology Conference (NSTC2007), University of Maryland, 19–21 June 2007.
[42] P. Rosch, M. Schmitt, W. Kefer and J. Popp, J. Mol. Struct. 661 (2003) p.363.
[43] R.M. Jarvis, A. Brooker and R. Goodacre, Anal. Chem. 76 (2004) p.5198.
[44] J.W. Schopf, A.B. Kudryavtsev, G.T. Agresti David, J. Wdowiak and A.D. Czaja, Nature 416 (2002) p.73.
[45] M. García-Ruiz, S.T. Hyde, A.M. Carnerup, A.G. Christy, M.J. Van Kranendonk and N.J. Welham, Science 302 (2003) p.1194.
[46] M.D. Brazier, O.R. Green, A.P. Jephcoat, A.K. Kleppe, M.J. Van Kranendonk, J.F. Lindsay, A. Steele and N.V. Grassineauk, Nature 416 (2002) p.76.
[47] G.J. Thomas Jr. and A.H. Wang, *Laser Raman spectroscopy of nucleic acids*, in *Nucleic Acids and Molecular Biology*, F. Eckstein and D.M.J. Lilley, eds., Springer, Berlin, 1988, p.1.

[48] C.P. McKay, E.I. Friedmann, B. Gomez-Silva, L. Cáceres-Villanueva, D.T. Andersen and R. Landheim, Astrobiology 3 (2003) p.393.
[49] R. Navarro-González, F.A. Rainey, P. Molina, D.R. Bagaley, B.J. Hollen, J. de la Rosa, A.M. Small, R.C. Quinn, F.J. Grunthaner, L. Cáceres, B. Gomez-Silva and C.P. McKay, Science 302 (2003) p.1018.
[50] K.A. Warren-Rhodes, K.L. Rhodes, S.B. Pointing, S.E. Ewing, D.C. Lacap, B. Gómez-Silva, R. Amundson, E.I. Friedmann and C.P. McKay, Microb. Ecol. 52 (2006) p.389.
[51] E.E. Brabb, R.W. Graymer and D.L. Jones, Geology of the onshore part of San Mateo County, California: a digital database. USGS, Open-File Report, 1998, p.98. Available at: http://pubs.usgs.gov/of/1998/of98-137/smgeo.txt.
[52] H.G.M. Edwards, S.E.J. Villar, J. Parnell, C.S. Cockell and P. Lee, Analyst 130 (2005) p.917.
[53] S.A. Benner, K.G. Devine, L.N. Matveeva and D.H. Powell, Proc. Natl. Acad. Sci. USA 97 (2000) p.2425.
[54] J. Eigenbrode, L.G. Benning, J. Maule, N. Wainwright, A. Steele, H.E.F. Amundsen and the AMASE, Astrobiology 9 (2006) p.455.
[55] C.C. Allen, N.R. Wainwright, S.E. Grasby, R.P. Harvey, *Life in the Ice. Sixth International Conference on Mars*, 2003, contribution no. 3138.
[56] S.E. Haydel, C.M. Remenih and L.B. Williams, J. Antimicrob. Chemother. 61 (2008) p.353.
[57] L.B. Williams, M. Holland, D.D. Eberl, T. Brunet and L.B. de Courssou, Miner. Soc. Bull. (Lond.) 139 (2004) p.3.
[58] W.A. Nolte, *Oral Microbiology*, Vol. 4, Mosby, London, 1982, p.3.
[59] J.R. Rogers and P.C. Bennett, Chem. Geol. 203 (2004) p.91.
[60] S.A. Ewing, B. Sutter, J. Owen, K. Nishiizumi, W. Sharp, S.S. Cliff, K. Perry, W. Dietrich, C.P. Mckay and R. Amundson, Geochim. Cosmochim. Acta 70 (2006) p.5293.
[61] B. Sutter, J.B. Dalton, S.A. Ewing, R. Amundson and C.P. Mckay, J. Geophys. Res. 112 (2007) p.0148.
[62] S. Guggenheim and R.T. Martin, Clays Clay Miner. 43 (1995) p.255.
[63] US Department of Agriculture, *Field Book for Describing and Sampling Soils*, Vol. 2.0, USDA, Washington, DC, 2002.
[64] M. Goman, F. Malamud-Roam and B.L. Ingram, J. Coast. Res. 24 (2008) p.1126.